Atomistic Calculations of Phonon Frequencies and Thermodynamic Quantities for Crystals of Rigid Organic Molecules

Graeme M. Day,[†,§] Sarah L. Price,[*,†] and Maurice Leslie[‡]

Centre for Theoretical and Computational Chemistry, Department of Chemistry, University College London, 20 Gordon Street, London, WC1H 0AJ, United Kingdom, and CCLRC Daresbury Laboratory, Daresbury, Warrington, WA4 4AD, United Kingdom

Received: April 25, 2003; In Final Form: June 20, 2003

Rigid-body, $\mathbf{k} = 0$ phonon frequencies have been calculated within the crystal structure modeling program DMAREL, enabling the use of anisotropic atom−atom model potentials. Five organic crystals (hexamethylenetetramine, naphthalene, pyrazine, imidazole, and α-glycine) were chosen to sample a range of intermolecular interactions for determining the sensitivity of the calculated frequencies to changes in the empirical repulsion-dispersion parameters and the electrostatic model. A carefully parameterized simple exp-6 model can describe vibrations in simple van der Waals crystals and some hydrogen bonded crystals reasonably well. However, for weaker polar interactions, an accurate model of the electrostatics is needed. Bending of weak polar interactions and shearing of close contacts with delocalized π-systems are particularly sensitive to the description of electrostatic interactions. Point charge models generally underestimate the resistance to deforming hydrogen bonds, and a distributed multipole model stabilizes these interactions. Because of their statistical nature, vibrational contributions to the energy can be estimated more accurately than the frequencies of individual modes, and the best models give good estimates of zero-point energies and the vibrational partition function, which should be useful in predicting the relative stability of polymorphs.

Introduction

Pharmaceutical scientists require an understanding of the thermodynamic properties of the different polymorphic forms of crystalline pharmaceuticals,[1,2] lest a phase transformation should occur during manufacture or storage. Indeed, the temperature−pressure behavior, and the possibility of a change of polymorphic form, is a major issue in the development of all molecular crystalline materials.[3] The vibrational properties of crystals are responsible for much of their thermal behavior, such as expansion, polymorphic phase transitions, and, eventually, melting. Since kinetic factors can hinder the experimental observation of phase transformations, or even the discovery of the most stable polymorph,[4] computational studies of the organic solid state have considerable potential for benefiting the development of novel organic materials.

Our main motivation for this study of phonon calculations is to examine the vibrational contributions to the crystal energy, which has been included in studies of the relative stability of polymorphs and predicted crystal structures.[5−10] Gavezzotti and Filippini[5] calculated energy differences in 204 pairs of polymorphs, including the vibrational entropy calculated from rigid-body harmonic frequencies using the UNI model potential,[11,12] and showed that the entropy differences were generally small (<15 J/mol·K). However, they can become significant when compared with the small lattice energy differences that are often calculated between known and hypothetical crystal structures.[6] Hence, recent crystal structure prediction studies have included vibrational contributions in the thermodynamic ranking of proposed structures.[7−10] It is apparent that temperature effects may often be important in computational polymorph prediction,[13] so an assessment of the sensitivity of such calculations to the form and parameterization of the model potential is necessary. We have calculated the intermolecular $\mathbf{k} = 0$ frequencies and their contributions to the crystals' energies, as these modes are most easily compared with experimental frequencies, so errors in the calculations are easily estimated. Off zone center modes will be required for accurate thermodynamical calculations and for identifying unstable structures, such as the imaginary modes at $\mathbf{k} = 1/2$ that point to cell doubling.[14] These are likely to be similarly affected by the approximations considered as the $\mathbf{k} = 0$ modes. By treating the molecules as rigid bodies, we ignore the intramolecular modes, which are not expected to vary significantly across polymorphs of small molecules. Furthermore, since previous lattice dynamical studies of molecular crystals have studied only one molecule or a closely related family of molecules, we have studied a set of molecules chosen to test a range of types and strengths of intermolecular interactions.

Phonon frequencies, and the corresponding motions, are determined by the forces between molecules, and hence the choice of intermolecular potential is a key factor in the accuracy of calculations. Indeed, while the ability of a given potential to model the solid state is often judged on how well structural parameters and lattice energies are reproduced, the computation of vibrational properties of crystals has sometimes been used in the refinement of model intermolecular potentials[15,16] and is useful for evaluating existing models. In a previous study,[17] we examined how calculations of a related property, the elastic constants, are affected by changes in the intermolecular potential.

* Corresponding author. Fax 44-20-7679-7463. E-mail s.l.price@ucl.ac.uk.
† University College London.
‡ CCLRC Daresbury Laboratory.
§ Current address: Department of Chemistry, University of Cambridge, Lensfield Road, Cambridge, CB2 1EW, United Kingdom.

10.1021/jp035125f CCC: $25.00
Published on Web 09/06/2003

TABLE 1: Molecules Studied, Experimental Crystal Structures, and Observed Lattice Frequencies[a]

Molecule, Crystal Structure, and CSD REFCODE	Molecular Structure	Space Group	Experimental Spectra and Number of Optic Modes	Previous Calculated Spectra
hexamethylenetetramine REF: HXMTAM10[18] T = 15 K, Neutron		$I\bar{4}3m$ (Z' = 1/12)	3 (degenerate) modes T = 100K, 298K[19] (INS)	Dolling and Powell,[19] Cochran and Pawley ,[20] Powell and Sándor[21]
naphthalene REF: NAPHTHA14[22] T = 12K, Neutron		$P2_1/c$ (Z' = ½)	9 modes T = 6K, perdeuterated[23] (INS)	Pawley et al,[24-27] Della Valle *et al*,[28] Righini *et al*,[29,30] Jindal and Kalus,[31,32] Pertsin *et al*[33]
pyrazine REF: PYRAZI[34] Room Temp. REF: PYRAZI01[35] T = 184K, X-Ray		*Pmnn* (Z' = ¼)	9 modes T = 77K[36] (IR) T = 4.2, 300K[37] (Raman) Room Temp., perdeuterated[38] (INS)	Ito and Shigeoka,[39] Reynolds,[38] Gamba *et al*[40,41]
imidazole REF: IMAZOL06[42] T = 103K Neutron		$P2_1/c$ (Z' = 1)	21 modes T = 93K[43] (IR) T = 100K[44] (Raman)	
α-glycine REF: GLYCIN05[45] T = 295K Neutron	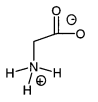	$P2_1/n$ (Z' = 1)	21 modes Room Temp.[46,47] (Raman and IR)	Machida *et al*[46,47]

[a] IR = Infrared, INS = Inelastic Neutron Scattering.

Here, we test the same set of model potentials, with point charge and distributed multipole models of electrostatic interactions, for their ability to reproduce observed phonon frequencies.

Methods and Computational Details

A test set of five representative rigid molecules (Table 1) was chosen from the restricted set of organic molecules where a low-frequency spectrum of sufficient quality could be found in the literature.

Naphthalene was chosen as an example of a weak, van der Waals crystal, where the electrostatic contribution to the lattice energy is relatively small. The pyrazine and hexamethylenetetramine crystals are, again, dominated by the weak van der Waals interactions, but local polarity in the molecules increases the importance of the electrostatic interactions. Many important molecular organic crystals are held together in hydrogen bonding networks, so we have chosen two molecular crystals with different hydrogen bonding strengths and patterns − imidazole and glycine. The second of these is zwitterionic in the crystalline phase, so the nonbonded interactions are strong, and more characteristic of molecular salts than neutral molecules.

For small organic molecules, there is usually a significant difference in the strengths of inter- and intramolecular interactions, and we treat the molecules as rigid building blocks of the crystal lattice. We have used this rigid-body approximation in all of our calculations and fixed the molecular geometry from the experimentally determined crystal structure, from the results of neutron diffraction studies, where available. The X-ray molecular structure of pyrazine had the C−H bond lengths adjusted to 1.08 Å.[48]

Model Potentials. The reliability of any molecular simulation depends on how realistically the form and parameterization of the model intermolecular potential reproduces intermolecular interactions in the crystal. Model potentials for typical organic molecules are still largely empirical[49] and based on the pairwise additive atom−atom potential method, which has been the basis of modeling many crystal properties.[33] Thus exchange-repulsion and dispersion contributions to the intermolecular energy, as a function of separation, R, and relative orientation, Ω, are modeled by

TABLE 2: Buckingham (exp-6) Potential Parameters, $U_{rep-disp}(R_{ik}) = A_{\iota\kappa}\ \exp(-B_{\iota\kappa}R_{ik}) - C_{\iota\kappa}R_{ik}^{-6}$

potential[a]	atom pair	A (kJ/mol)	B (Å^{-1})	C (Å^{6}kJ/mol)	R_e (Å)[b]	ϵ (kJ/mol)[b]
FIT	C···C (W81)[50,51]	369743	3.60	2439.8	3.90	0.398
	N···N (W84)[52]	254529	3.78	1378.4	3.66	0.324
	O···O (W81)[51]	230064	3.96	1123.6	3.41	0.400
	H_C···H_C(W84)[50]	11971	3.74	136.4	3.31	0.053
	H_N···H_N (FIT)[53]	5030	4.66	21.5	2.48	0.044
	H_O···H_O (FIT)[54]	2263	4.66	21.5	1.94	0.135
W99 [55−57]	C(4)···C(4)	131571	3.60	978.36	3.83	0.175
	C(3)···C(3)	270363	3.60	1701.73	3.92	0.268
	H(1)···H(1)(H_C)[c]	12680	3.56	278.37	3.23	0.117
	H(2)···H(2) (H_O)[c]	361.3	3.56	0.0		
	H(4)···H(4) (H_N)[c]	764.9	3.56	0.0		
	N(2)···N(2)	102369	3.48	1398.15	3.72	0.283
	N(3)···N(3)	191935	3.48	2376.55	3.78	0.443
	N(4)···N(4)	405341	3.48	5629.82	3.71	1.157
	O(1)···O(1)	241042	3.96	1260.73	3.37	0.475
	O(2)···O(2)	284623	3.96	1285.87	3.45	0.431
UNI[11,12]	C···C	226145	3.47	2418.4	3.89	0.387
	N···N	365263	3.65	2891.1	3.70	0.629
	O···O	195309	3.74	1334.7	3.61	0.336
	H···H	24158	4.01	109.2	3.36	0.042
	C···N	491494	3.86	2790.7	3.49	0.851
	C···O	393087	3.74	2681.9	3.61	0.674
	C···H	120792	4.10	472.8	3.29	0.205
	N···O	268571	3.86	1523.0	3.50	0.464
	N···H	228279	4.52	502.1	2.98	0.394
	(N-)H···N	7547601	7.37	690.4	1.90	8.42

[a] The W81, W84, and W99 parameters were fitted in combination with an atomic point charge model, the additional FIT parameters with a DMA model, and the UNI parameters with no electrostatic model. In W99, C(3) and C(4) represent three- and four-coordinated carbon atoms, H(1) is bonded to carbon, H(2) is an alcoholic hydrogen and H(4) is bonded to nitrogen, N(2) has no bonded hydrogen atoms, N(3) has one bonded hydrogen and N(4) has two or more bonded hydrogen atoms, O(1) is bonded to one atom and O(2) is bonded to two other atoms. [b] R_e is the exp-6 potential minimum and ϵ is the potential well depth. [c] For W99 calculations, the center of the potential is shifted off the nuclear sites for hydrogen atoms, by 0.1 Å toward the heavy atom to which it is bonded. Point charge and distributed multipole interaction sites remained coincident with the nuclei.

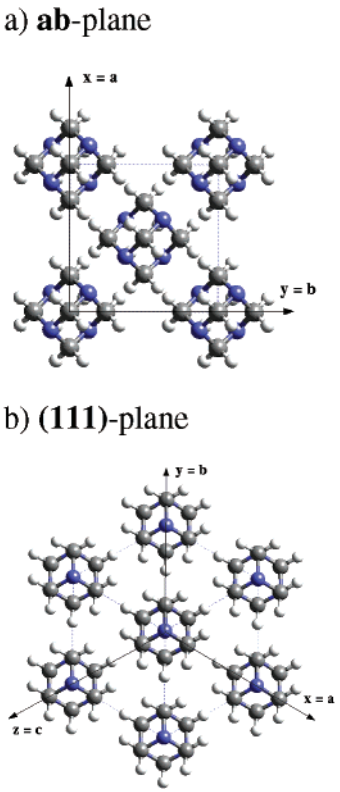

Figure 1. Crystal structure of hexamethylenetetramine. Figures prepared using the Cerius2 software.[73]

$$U_{\text{rep-disp},MN}(R,\Omega) = \sum_{i\in M,k\in N} U_{\text{rep-disp},ik}(R_{ik}) = \sum_{i\in M,k\in N} A_{\iota\kappa}\exp(-B_{\iota\kappa}R_{ik}) - \frac{C_{\iota\kappa}}{R_{ik}^6} \quad (1)$$

where i and k are the constituent atoms of molecules M and N, respectively, and the subscripts ι and κ identify the atom types of atoms i and k. Here, we have investigated three of the many available sets of general, transferable exp-6 parameters developed for modeling crystalline organic molecules (Table 2).

Two of the sets of repulsion−dispersion terms were parameterized in conjunction with an explicit model for the electrostatic forces, and assume the combining rules

$$A_{\iota\kappa} = \sqrt{A_{\iota\iota}A_{\kappa\kappa}}$$
$$B_{\iota\kappa} = \frac{B_{\iota\iota} + B_{\kappa\kappa}}{2}$$
$$C_{\iota\kappa} = \sqrt{C_{\iota\iota}C_{\kappa\kappa}} \quad (2)$$

to generate the heteroatomic potentials from the homoatomic parameters. The first set, denoted FIT, has been developed from the parameter sets originally fitted to the crystal structures and lattice energies of oxohydrocarbons (W81)[51] and azahydrocarbons (W84),[52] and later extended with polar hydrogen atom (H_O, H_N) parameters fitted to a large set of hydrogen-bonded organic molecules using a distributed multipole electrostatic model.[53,54] The second potential, W99, which distinguishes atom types for C, N, and O on bonding environment, was recently parameterized to a larger collection of hydrocarbon,[55] oxohydrocarbon,[57] and azahydrocarbon[56] crystal structures and lattice energies.

We consider two electrostatic models, both derived from an MP2(full)/6-31G(d,p) wave function of the isolated molecule, calculated within the Gaussian 98 suite of electronic structure programs.[58] Atomic point charges are the simplest, least computationally expensive approach, and we have calculated electrostatic potential (ESP) derived charges via the CHelpG[59] algorithm, as implemented in Gaussian 98,[58] constrained to reproduce the molecular dipole moment and preserve any molecular symmetry. Since some features of the electrostatic potential, e.g., from localized lone pairs and π-electron density, cannot be adequately described by a spherical atom model, we also use a more accurate representation of the electron density in terms of atom-centered multipoles, i.e., a charge, dipole, quadrupole, octupole, and hexadecapole at each nucleus. These were obtained by a distributed multipole analysis (DMA)[60,61] of the charge density.[62] The mechanics of the anisotropic electrostatic interactions[63−65] are implemented in the program DMAREL[65] for modeling crystals of rigid molecules. The electrostatic contributions to the lattice energy were evaluated by the Ewald summation technique[66] for charge−charge, charge−dipole, and dipole−dipole terms. All higher order electrostatic interactions, up to R^{-5} in the multipole expansion, were summed to a 15 Å cutoff between the centers of mass of the molecules.

The third potential (UNI) was developed assuming that all contributions to the intermolecular interaction could be described by the exp-6 potential. The parameters were fitted to the structures and sublimation energies of a large set of monofunctional organic molecular crystals,[11,12] abandoning the combining rules for heteroatomic interactions to allow the electrostatic effects to be absorbed as efficiently as possible into the exp-6 parameters. The resulting potentials have vastly different well depths, ϵ, and equilibrium distances, R_e, (Table 2) from models derived with an explicit electrostatic model.

Phonon Calculations. The theory behind the computation of phonon frequencies is given in many texts (e.g., Born and Huang,[67] Walmsley,[68,69] Califano,[70] and Dove[71]), so only brief details are needed here. In the rigid molecule approximation, each molecule is assigned a fixed axis system, with the origin at the center of mass and the axes pointing along the principal inertial axes.[69,70] Now, standard lattice dynamical theory leads to the following equation to describe the vibrations in a periodic

TABLE 3: Experimental and Calculated Crystal Structures and Energies of Hexamethylenetetramine[a]

structure	$-\Phi_{\text{latt}}$ (kJ/mol)[a]	$a = b = c$ (Å)	V (Å^3)
experimental[18]	79.9 ± 2.9	6.927	332.4
UNI	96.57	*−1.45%*	*−4.32%*
W84 + ESP	78.87	*+1.25%*	*+3.76%*
W99 + ESP	76.44	*+0.13%*	*+0.40%*
W84 + DMA	84.08	*+1.26%*	*+3.82%*
W99 + DMA	81.59	*+0.22%*	*+0.66%*

[a] The experimental lattice energy, $-\Phi_{\text{latt}}$, is approximated by $\Delta H^\circ_{\text{sub}} + 2RT$ at 298 K.[74]

TABLE 4: Harmonic and Quasi-Harmonic (100 K and 298 K) k = 0 Librational Lattice Frequency of Hexamethylenetetramine[a]

expt[19]	UNI	W84+ESP	W99+ESP	W84+DMA	W99+DMA
100 K	fully relaxed lattice				
63.7 (±2)	95.3	78.8	74.1	66.4	56.6
	100 K fixed lattice (**a** = 6.949Å)				
	74.1	87.0	72.7	73.7	56.1
298 K	298 K fixed lattice (**a** = 7.024Å)				
58.4 (±2)	62.8	77.0	64.9	64.9	50.2

[a] Frequencies in cm^{-1}.

TABLE 5: Experimental and Calculated Crystal Structures and Energies and Molecular Displacements for Naphthalene[a]

(a) Crystal Structures and Energies for Naphthalene

structure	$-\Phi_{latt}$[b] (kJ/mol)	A (Å)	b (Å)	c (Å)	β (degrees)	Vol (Å^3)	RMS error[c]
expt 239 K[80]	77.3 ± 2	8.21	5.97	8.68	123.4	355.3	
expt 12 K[22]		8.10	5.94	8.65	124.6	342.3	
UNI	73.42	*−3.95%*	*−0.15%*	*−1.03%*	*−4.15%*	*+0.45%*	2.36%
W81+ESP	70.15	*−0.18%*	*+2.92%*	*+0.89%*	*−1.95%*	*+6.59%*	1.77%
W99+ESP	64.68	*+0.38%*	*+1.98%*	*+0.73%*	*−1.75%*	*+5.77%*	1.24%
W81+DMA	73.84	*+3.44%*	*−0.13%*	*+1.17%*	*−1.17%*	*+6.33%*	2.10%
W99+DMA	68.78	*+4.63%*	*−1.62%*	*+1.12%*	*−0.88%*	*+5.44%*	2.90%

(b) Molecular Displacements of Naphthalene During Lattice Energy Relaxation

	fully relaxed			fixed cell[d]
structure	RMS translation (Å)[e]	RMS rotation (deg.)	F	RMS rotation (deg.)
UNI	0.15	5.12	52.29	2.20
W81+ESP	0.08	3.27	18.57	2.39
W99+ESP	0.19	2.57	14.49	2.05
W81+DMA	0.11	1.94	17.63	1.98
W99+DMA	0.14	2.51	30.13	1.57

[a] Calculated lattice parameters given as % deviations, 100 × (calc − expt)/expt, from the 12 K experimental structure (ref 22). In Table 5(b), displacements are relative to the 12 K experimental structure. [b] The experimental value is $\Delta H_{sub}+2RT$, averaged over 10 measurements at 298 K.[81−88] [c] Root-mean-square % error in lengths of lattice vectors **a**, **b** and **c**. [d] Translations are zero by symmetry in the fixed unit cell. [e] Root-mean-square change of center of mass position on minimization, defined relative to the origin of the unit cell.

lattice

$$\omega^2(\mathbf{k})w_\tau(M|\mathbf{k}) = \sum_{\tau',N} D^{MN}_{\tau\tau'}(\mathbf{k})w_{\tau'}(N|\mathbf{k}) \quad (3)$$

where $\omega(\mathbf{k})$ is the angular frequency ($2\pi \times$ frequency) of the vibration at wavevector $\mathbf{k}$, w_τ(N) is a mass-weighted displacement of molecule N along τ, a molecular displacement ($\tau = 1-3$) or torque ($\tau = 4-6$). $\boldsymbol{D}^{MN}_{\tau\tau'}(\mathbf{k})$ is the dynamical matrix defined by

$$\boldsymbol{D}^{MN}_{\tau\tau'}(\mathbf{k}) = (\mathrm{M}_{\tau,M}\mathrm{M}_{\tau',N})^{-(1/2)}\sum_{l'}\Phi^{0l'}_{\tau\tau'}(MN)\exp(i\mathbf{k}\cdot\mathbf{r}^{l'}) \quad (4)$$

Here, **M** are the molecular masses ($\tau = 1-3$) and moments of inertia ($\tau = 4-6$) and $\Phi^{0l'}_{\tau\tau'}(MN)$ is the matrix of second derivatives with respect to the displacements of molecule M (in the reference unit cell) and molecule N (in unit cell l') along τ and τ', respectively. The vector $\mathbf{r}^l$ joins the origins of the reference unit cell and unit cell l.

For each molecule, we started with the experimental crystal structure and used a modified Newton−Raphson procedure, using analytical forces, rigid body torques, and strain derivatives of the unit cell,[65] to locate a stationary point on the potential energy surface. The minimization path was constrained to the observed symmetry of the crystal, and eigenvalues of the Hessian were calculated at the resulting stationary point. Where a negative eigenvalue was found, the symmetry was lowered to a subgroup of the original spacegroup and the minimization was started along the path of the unstable eigenvector. For harmonic (stress-free) phonon calculations, the unit cell was varied within the minimization procedure until strain derivatives vanished. We also performed quasi-harmonic phonon calculations, with the unit cell fixed at the experimental structure and only internal degrees of freedom (i.e., molecular displacements and rotations) relaxed. The Hessian, $\Phi^{ll'}_{\tau\tau'}(MN)$, was evaluated numerically from the analytical gradients and its eigenvalues used to confirm that a minimum on the energy surface had been found. The rotational components of the second derivatives required for the dynamical matrix must be about the principal inertial axes, so a change of molecular axis system is required, from the Cartesian axes used in the definition of the multipole moments and the analytical gradients. These axes and gradients are rotated into the principal axis frame before numerical differencing for the second derivatives. From the numerical Hessian, the dynamical matrix, $\boldsymbol{D}^{MN}_{\tau\tau'}(\mathbf{k})$ in eq 4, was calculated for $\mathbf{k} = 0$, for comparison with the experimental frequencies. Splitting of the transverse and longitudinal zone-center modes (LO−TO splitting) is ignored here because it is expected to be small for charge neutral molecules and comparisons are made to experimental observations where the crystal orientation is often not specified. Nontrivial solutions of eq 3 were determined by solving the eigenvalue equations

$$|\boldsymbol{D}^{MN}_{\tau\tau'}(\mathbf{k}) - \omega^2(\mathbf{k})\delta_{\tau\tau'}\delta_{MN}| = 0 \quad (6)$$

from which the corresponding eigenvectors were also calculated to analyze the molecular motions corresponding to each mode. In-house software RUDOLPh[72] was used to visualize the vibrational modes, and their qualitative descriptions are given in the supplementary information.

Results

Hexamethylenetetramine(-d_{12}), $C_6N_4D_{12}$. Hexamethylenetetramine is a highly symmetric (T_d) molecule which crystallizes with unusually high symmetry ($I\bar{4}3m$, Figure 1) for an organic molecule, simplifying the relationship between model potential and calculated properties. The shortest intermolecular contacts (C−H···H−C at just under 2.7 Å and C−H···N at about 2.8 Å) are greater than the sum of van der Waals radii, so are not expected to be particularly strong. However, the sum of these weak interactions provides enough anisotropy in the molecule−molecule interactions to keep the crystal orientationally ordered up to at least 340 K.[19]

The 15 K neutron crystal structure[18] is reproduced satisfactorily using all model potentials (Table 3), with W99 being the most accurate, almost independent of the electrostatic model.

There is only one (triply degenerate) optic intermolecular mode, at approximately 60 cm^{-1}, which has been studied via coherent inelastic neutron scattering at 100 K (63.7 cm^{-1}) and 298 K (58.4 cm^{-1}).[19] The large gap between the frequency of the librational mode and our lowest calculated intramolecular mode (375.6 cm^{-1}, MP2/6-31G(d,p)) justifies our use of the

TABLE 6: Harmonic and Quasi-Harmonic k = 0 phonon frequencies for $C_{10}D_8$

(a) Harmonic **k** = 0 Phonon Frequencies Calculated for $C_{10}D_8$ at the Minimum in Φ_{latt}, in cm^{-1}

mode	expt (6 K)	UNI	W81 + ESP	W99 + ESP	W81 + DMA	W99 + DMA
			translational modes			
ν_7 (A_u)	57.7	46.9	46.5	45.4	50.5	49.3
ν_9 (B_u)[a]		63.1	58.8	57.3	66.5	65.5
(H_8, 4.7K)	79	65.1	60.7	59.1	68.6	67.5
ν_8 (A_u)	107.1	120.0	112.9	105.8	111.2	104.4
			librational modes			
ν_4 (B_g)	54.0	52.6	51.6	47.6	45.5	41.6
ν_1 (A_g)	64.4	63.9	52.2	51.6	51.2	46.2
ν_5 (B_g)	79.4	87.7	77.4	71.3	77.4	71.8
ν_2 (A_g)	83.7	99.6	92.0	86.1	94.1	89.0
ν_3 (A_g)	112.4	147.2	137.0	126.5	143.7	133.9
ν_6 (B_g)	130.1	144.9	139.6	129.0	140.4	132.0

b. Quasi-Harmonic **k** = 0 Phonon Frequencies Calculated for $C_{10}D_8$ Using Fixed (experimental, 12 K[22]) Lattice Vectors, in cm^{-1}

mode	Expt (6K)	UNI	W81 + ESP	W99 + ESP	W81 + DMA	W99 + DMA
			translational modes			
ν_7 (A_u)	57.7	54.3	62.3	57.1	63.5	59.8
ν_9 (B_u)[a]		69.5	77.1	71.5	79.9	74.4
(H_8, 4.7K)	79	71.7	79.5	73.7	82.4	76.7
ν_8 (A_u)	107.1	119.4	142.6	131.0	145.1	133.8
			librational modes			
ν_4 (B_g)	54.0	53.9	65.0	59.6	62.8	57.5
ν_1 (A_g)	64.4	65.1	71.0	63.2	67.0	58.2
ν_5 (B_g)	79.4	89.4	96.8	87.1	97.5	87.4
ν_2 (A_g)	83.7	108.3	119.6	108.8	122.3	111.4
ν_3 (A_g)	112.4	143.3	170.3	153.6	171.2	153.1
ν_6 (B_g)	130.1	144.6	172.6	157.8	175.1	159.8

[a] The zone-center frequency of the B_u (ν_9) mode was not reported by Sheka et al,[23] so the 4.7K frequency for $C_{10}H_8$[90] is included, along with the calculated ν_9 frequencies for the undeuterated crystal.

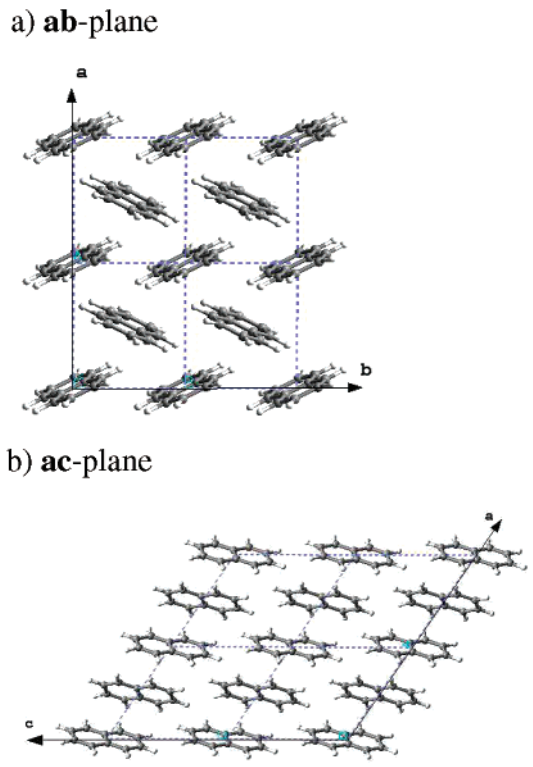

Figure 2. Crystal structure of naphthalene.

rigid body formalism. While the frequency calculated with the UNI potential is about 50% too large (Table 4), those calculated using an explicit electrostatic model are much closer to the observed frequency. In contrast to the sensitivity of the structure to the model potential, the frequency shift caused by replacing point charges with distributed multipoles is comparable to that associated with changing the exp-6 parameters. Some of these effects are due to the differences in relaxed lattice parameters. The equilibrium (0 K) lattice of the W84 models nearly corresponds to room temperature (**a** = 7.024 Å), while the W99 equilibrium lattice corresponds approximately to 50 K observations (**a** = 6.934 Å). As the lattice frequency increases by almost 8% from room temperature to 100 K, the effects of small changes (<1%) in the lattice are significant.

This was confirmed by the calculation of the quasi-harmonic frequencies (Table 4), at both room temperature, using the corresponding lattice parameter,[75] and at 100 K, where the lattice parameter was obtained by interpolating between the six structures covering the range 15−200 K.[18] At both temperatures, the effects of the exp-6 parameters and the electrostatic model are comparable. Exchanging W84 for W99 or point charges for a DMA decreases the frequency by approximately 15 cm^{-1} at both temperatures, generally improving the comparison with experiment. The W99+DMA model reproduces the temperature shift (about 5 cm^{-1} from 100 K to room temperature) most accurately.

Naphthalene, $C_{10}D_8$. The naphthalene crystal is dominated by van der Waals forces; calculations with our most accurate electrostatic model estimate that the electrostatic contribution is 11−13% of the total lattice energy. Because of the relative simplicity of the model potential for hydrocarbons, the vibrational spectrum of naphthalene has been studied extensively by computational methods (e.g., refs 24, 28, 33, 76). The molecules lie on crystallographic inversion centers in the monoclinic space group $P2_1/c$ ($Z = 2$), so the translational and librational motions cannot mix. The structure and spectra have been studied at a range of pressures and temperatures[23,77] and we chose the most recent low-temperature data[23] on fully deuterated naphthalene for our comparisons.

The calculated lattice energies agree with the observed

TABLE 7: Experimental and Calculated Crystal Structures and Energies and Molecular Displacements of Pyrazine

(a) Experimental and Calculated Crystal Structures and Energies for Pyrazine[a]

structure	$-\Phi_{latt}$ (kJ/mol)	*a* (Å)	*b* (Å)	*c* (Å)	vol (Å^3)	RMS error[c]
expt (RT)[34]	61.3 ± 0.5 [b,91]	9.32	3.82	5.91	210.1	
expt (184 K)[35]		9.32	3.73	5.85	203.6	
UNI	61.3	*+1.86%*	*−0.82%*	*−8.08%*	*−7.20%*	4.81%[d]
W84+ESP	53.2	*−19.27%*	*−1.17%*	*+29.23%*	*+2.14%*	20.22%[d]
W99+ESP	49.5	*−9.56%*	*+2.21%*	*+13.11%*	*+0.45%*	9.45%[d]
W84+DMA	54.3	*+3.67%*	*+0.77%*	*−2.49%*	*+1.88%*	2.60%
W99+DMA	54.6	*+2.32%*	*+2.60%*	*−5.43%*	*−0.72%*	3.72%

(b) Molecular Displacements of Pyrazine During Lattice Energy Relaxation

	fully relaxed			fixed cell [e]
	RMS translation (Å) [f]	RMS rotation (deg.)	*F*	RMS rotation (deg.)
UNI	0.20	15.25	136.6	17.28
W84+ESP	0.84	47.87	1931.6	18.84
W99+ESP	0.58	61.81	1517.0	43.35
W84+DMA	0.13	2.07	23.1	1.89
W99+DMA	0.14	5.14	50.2	0.37

[a] Calculated lattice parameters given as % deviations, 100 × (calc − expt)/expt, from experimental values. [b] The experimental value is $\Delta H_{sub}+2RT$. [c] Root-mean-square % error in lengths of lattice vectors *a*, *b*, and *c*, compared to 184 K structure. [d] The original symmetry is lost and final ($P2_1/c$) structure has $\alpha = 87.73°$ (UNI), $\alpha = 82.21°$ (W84+ESP), $\alpha = 73.89°$ (W99+ESP). [e] Translations are zero by symmetry in the fixed unit cell. [f] Root-mean-square change of center of mass position on minimization, defined relative to the origin of the unit cell.

enthalpy of sublimation at 298 K, within expected differences[78] (Table 5a). The reproduction of the cell parameters at $T = 12$ and 239 K by the fully relaxed structures (Table 5a) does not distinguish between the potentials as much as the molecular translations and rotations away from the experimental structure (Table 5b). The poorer performance of the UNI potential is obvious from the structural drift measure, *F*, calculated as[79]

$$F = (\Delta\theta/2)^2 + (10\Delta x)^2 + \sum_{\tau = a,b,c} (100\Delta\tau/\tau)^2 + \sum_{\chi = \alpha,\beta,\gamma} (\Delta\chi)^2 \quad (7)$$

where $\Delta\theta$ is the rigid-body rotation (in degrees) on lattice energy minimization, Δx is the rigid-body translation (Å), and $\Delta\tau$ and $\Delta\chi$ are the changes in the lattice parameters.

The models with point-charge electrostatics reproduce the structure quite well, and the distributed multipole representation of the electrostatics does not noticeably improve the structure. Previous studies have shown the importance of the molecular quadrupole in describing behavior of crystalline naphthalene,[29,33] and the atomic point charges are enough to reproduce this molecular moment adequately.[89]

The molecules are packed with tilted edge-to-face contacts (Figure 2) and the nine optic zone-center modes correspond to various distortions, including distortions of the edge-to-face interactions. RMS differences between calculated and observed ($T = 6$ K)[23] frequencies (Table 6a for fully relaxed structures and Table 6b for quasi-harmonic calculations) are nearly the same with all the model potentials. The DMA models represent the π-electrons most realistically and show a slight improvement over the rest in the low energy part of the spectrum, where the motions shear the edge-to-face contacts. The high-frequency modes are affected most by the exp-6 parameterization and the W99 potential shows better agreement with experiment than W84, particularly where H···H contacts are stretched (ν_2); here, the shift of the exp-6 site away from the hydrogen nuclei softens the mode significantly. The A_g/B_g split between the highest frequency librational modes (ν_3, ν_6) is poorly reproduced in the fully relaxed structures, and three of the five model potentials reverse the order of these modes. In the fixed experimental unit cell, both ν_3 and ν_6 are shifted too high, but all of the models now predict the correct order of the two highest modes. Overall,

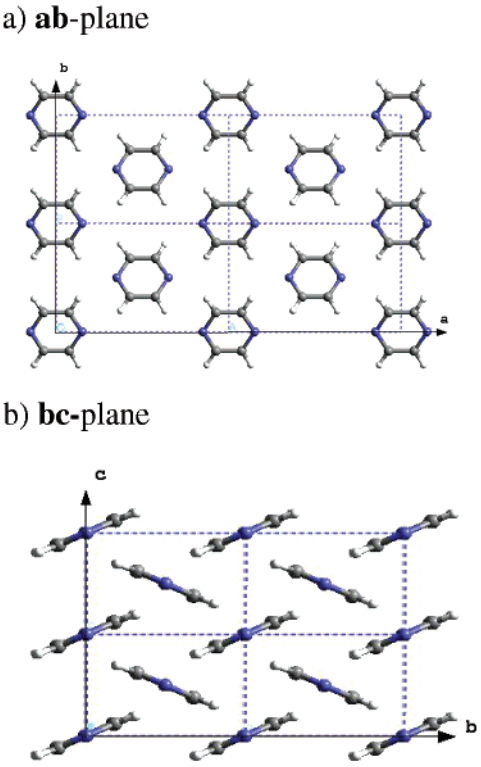

Figure 3. Crystal structure of pyrazine.

errors in the quasi-harmonically calculated frequencies are greater than when the external strains are relaxed and the large errors are mostly in the upper half of the spectrum.

Pyrazine, $C_4N_2H_4$. Pyrazine crystallizes with $Z' = 1/4$ ($Z = 2$) in the orthorhombic space group *Pmnn*, in which the N−N axes of all the molecules are aligned along the longest unit cell axis, **a**, and there is offset ring−ring stacking almost along **c**. The planes of molecules offset by $a/2$ form a 47° angle (Figure 3).

As with naphthalene, the symmetry of this molecular crystal simplifies the characterization of the experimental spectra. There are only nine optic modes in the vibrational spectrum (A_g, A_u, B_{1u}, $2\times B_{1g}$, B_{2u}, $2\times B_{2g}$, B_{3g}), and mixing of the translational and rotational vibrational motions is forbidden. The relaxed

TABLE 8: Harmonic and Quasi-harmonic k = 0 Phonon Frequencies Calculated for Pyrazine

(a) Harmonic **k** = 0 Phonon Frequencies Calculated for Pyrazine at the Minimum in Φ_{latt} (cm^{-1})

mode	expt. (low *T*)	W84+DMA	W99+DMA
		Translational Modes (77 K)	
$\nu_7(A_u)$	not observed	123.3	123.0
$\nu_8(B_{1u})$	54 (IR)	52.2	54.8
$\nu_9(B_{2u})$	79 (IR)	65.0	69.8
		Librational Modes (4.2K, Raman)	
$\nu_1(A_g)$	128	147.3	145.4
$\nu_2(B_{1g})$	57	54.2	64.8
$\nu_3(B_{1g})$	88	76.8	73.6
$\nu_4(B_{2g})$	58	48.1	51.1
$\nu_5(B_{2g})$	98	111.3	117.1
$\nu_6(B_{3g})$	136	161.1	161.3

(b) Quasi-harmonic **k** = 0 Phonon Frequencies Calculated for Pyrazine at the Fixed Room-Temperature Lattice (cm^{-1})

mode	expt (RT)	UNI	W84+ESP	W99+ESP	W84+DMA	W99+DMA
			Translational Modes			
$\nu_7(A_u)$	not observed	120.8 (d4)	137.0 (d4)	119.5 (d4)	141.5 (d4)	122.1(d4)
$\nu_8(B_{1u})$	48	53. 8 (d4)	64.7 (d4)	62.5 (d4)	69.1 (d4)	61.4 (d4)
$\nu_9(B_{2u})$	68	67.8 (d4)	75.7 (d4)	64.8 (d4)	70.1 (d4)	64.7(d4)
			Librational Modes			
$\nu_1(A_g)$	104	103.2	86.8	104.0	111.1	101.1
$\nu_2(B_{1g})$	46	**−62.4**	**−60.0**	**−73.7**	26.8	58.6
$\nu_3(B_{1g})$	72	97.1	82.7	104.2	90.4	67.4
$\nu_4(B_{2g})$	47	**−36.4**	**−30.4**	**−41.7**	10.2	27.6
$\nu_5(B_{2g})$	78	34.0	63.1	59.3	113.6	117.2
$\nu_6(B_{3g})$	115	115.6	106.9	122.7	138.7	129.4

[a] Room-temperature IR experimental frequencies for $C_4N_2H_4$ from ref 36 and 300 K Raman frequencies for $C_4N_2D_4$ from ref 37.

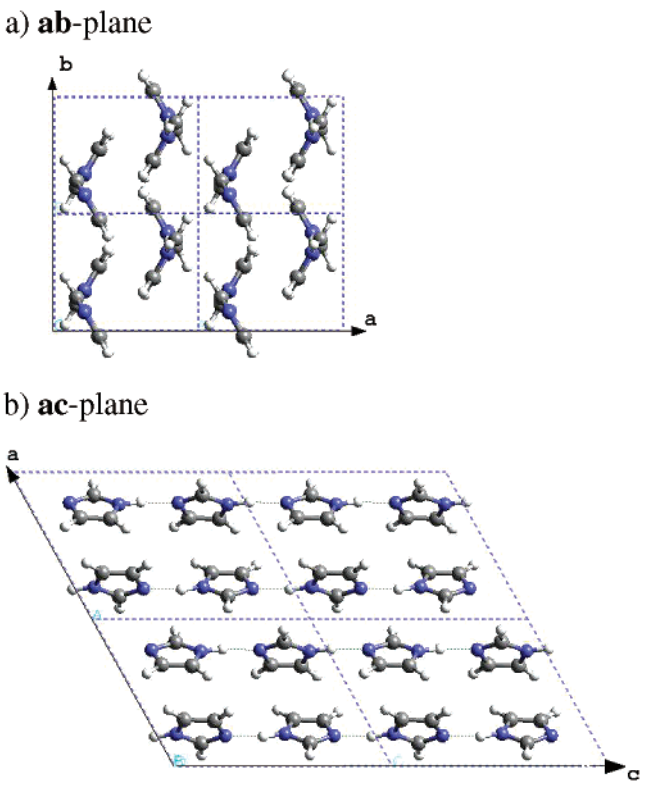

Figure 4. Crystal structure of imidazole. Hydrogen bonds are shown with fine dashed lines.

structures (Table 7a,b) show that the anisotropy of the electrostatic forces is very important in determining the structure of this crystal. From the DMA potentials, electrostatics contribute 35−40% (about 20 kJ/mol) of the total lattice energy, over two-thirds of which is associated with the anisotropic terms (charge-dipole and higher). All but the distributed multipole electrostatic models fail to reproduce the lattice structure satisfactorily, with large errors in the **a** and **c** lattice vectors and significant molecular reorientations. For these models, much of the crystal's symmetry has to be removed to find a stable minimum in the lattice energy. The DMA models reproduce the stacking distance of 2.33 Å to within 0.32 Å (W84+DMA) and 0.13 Å (W99+DMA), while the others expand this interaction by 0.9−1.2 Å. The orientation of the C−H···N interaction is poorly reproduced with the point charge models − the W84+DMA and W99+DMA model potentials reproduce the experimental C−H···N angle of 153° to within 3°, while the equilibrium angle is much too acute with the ESP models (106° with W84+ESP, 137° with W99+ESP). The UNI model reproduces the weak hydrogen bond adequately but fails to model the $\pi-\pi$ interaction properly.

These deficiencies are apparent in the quasi-harmonic room-temperature calculations with enforced *Pmnn* symmetry (Table 8), showing instabilities to molecular rotation (ν_2, ν_4). Thus only the DMA model harmonic frequencies can be compared to the low temperature experimentally determined frequencies (Table 8a).

Our results agree with earlier computational studies of the pyrazine crystal,[38,40,92] which found that C−H···N dipole−dipole interactions are necessary to describe the vibrations satisfactorily. The two modes (ν_2, ν_4) that are unstable in the quasi-harmonic calculations without anisotropic electrostatics are those for which Gamba and Bonadeo[40] found the electrostatic interactions to be most important. The restoring force for the C−H···N out-of-plane bending mode, ν_4, is almost entirely due to the orientational dependence of the interaction and the ν_2 vibration bends the C−H···N contacts in a similar manner, while also shearing the C−H···H−C contacts. When the lattice is allowed to relax, the weak hydrogen bond increases in strength due to the higher multipole interactions dominating over the loss of charge−charge contribution. For the fixed lattice used in the quasi-harmonic calculations, the weaker hydrogen bond produces modes that are too soft (except ν_2 with W99+DMA).

TABLE 9: Experimental and Calculated Crystal Structures and Energies and Molecular Displacements for Imidazole

(a) Experimental and Calculated Crystal Structures and Energies[a]

	$-\Phi_{latt}$[b] (kJ/mol)	*a* (Å)	*b* (Å)	c (Å)	β (deg)	vol (Å^3)	RMS error[c]
expt	88.1 ± 0.2	7.57	5.37	9.78	119.1	347.3	
UNI	59.07	+0.69%	−3.70%	+2.32%	+4.19%	−5.96%	2.55%
FIT + ESP	61.89	+2.78%	−1.25%	+2.49%	+0.61%	+3.28%	2.27%
W99 + ESP	59.25	+3.93%	−2.43%	+2.01%	−0.57%	+4.12%	2.91%
FIT + DMA	78.38	+1.96%	+1.78%	+0.30%	+1.28%	+2.51%	1.54%
W99 + DMA	79.32	+0.38%	+2.47%	−2.66%	−1.42%	+1.72%	2.11%

(b) Molecular Displacements During Lattice Energy Relaxation

	fully relaxed			fixed cell	
	RMS translation (Å)[d]	RMS rotation (deg.)	F	RMS translation (Å)	RMS rotation (deg.)
UNI	0.35	3.90	60.53	0.44	10.83
FIT+ESP	0.17	3.61	22.24	0.23	5.08
W99+ESP	0.23	2.64	33.04	0.17	3.08
FIT+DMA	0.13	4.08	15.32	0.14	3.87
W99+DMA	0.16	4.92	24.79	0.18	4.73

[a] Calculated lattice parameters given as % deviations, 100 × (calc − expt)/expt, from experimental values. [b] Experimental lattice energy taken as $-(\Delta H_{sub} + 2RT)$.[93] [c] Root-mean-square % error in lengths of lattice vectors **a**, **b** and **c**. [d] Root-mean-square change of center of mass position on minimization, defined relative to the origin of the unit cell.

The in-plane C−H···N bending modes (ν_3, ν_5) are reproduced quite well with distributed multipole electrostatics, but ν_5 is much too soft with the isotropic potentials, indicating that anisotropic electrostatics are important for in-plane bending as well. When C−H···N stretching as well as bending is involved (ν_8, ν_9), atom−atom anisotropy is less important. The exp-6 contributions to the dynamical matrix are dominant for the C−H···H−C stretching modes, ν_1 and ν_6,[40] and the W99 model, with improved aromatic carbon parameters and the shift of the hydrogen center of repulsion, gives noticeably better results than the W84 model.

Imidazole, $C_3N_2H_4$. Unlike pyrazine and hexamethylenetetramine, imidazole has polar hydrogen atoms to form hydrogen bonds to the lone pairs on the nitrogen atom. These form chains along the **c** axis of the monoclinic ($P2_1/c$, $Z = 4$) lattice (Figure 4). Adjacent molecules in the chains are twisted by about 60° with respect to each other, and these chains are joined by short (2.6 Å) C−H···N contacts. With these weak and strong hydrogen bonds forming a network through the crystal, the electrostatic interactions are dominant and our calculations (W99+DMA) estimate that the electrostatic contribution is about 60% of the total lattice energy.

The structures are moderately well reproduced by all of the model potentials (Table 9a,b). The FIT+DMA model gives the best results and reproduces the length and directionality of the N−H···N contacts to within 0.01 Å and 3°. Hydrogen bonding with the W99+DMA potential is exaggerated, shortening the strong hydrogen bond by 0.17 Å. The ESP models both elongate the hydrogen bond with respect to their DMA counterparts and also incorrectly predict a significant deviation from linearity. While the UNI potential retains the N−H···N linearity, it also elongates the intermolecular contact. All five models reproduce the length and orientation of the weaker C−H···N interaction reasonably well.

Calculated frequencies (Table 10a,b) are compared to the observed frequencies at the lowest available temperatures (100 K Raman and 93 K IR). The success of the simple exp-6 model (UNI) shows that the careful parameterization of an isotropic atom−atom potential can give quite good results. At the fully relaxed structures, the W99+DMA model exaggerates the hydrogen bond stretching (ν_{10}, ν_{16}) and high energy bending frequencies (ν_6, ν_{12}, ν_{17}, ν_{21}) because of the shortening of these interactions. However, in the quasi-harmonic calculations, the chain length is fixed by the length of the **c** axis and agreement with experiment is excellent. Many of the low energy hydrogen bond bending modes (ν_2, ν_4, ν_8, ν_9, ν_{13}, ν_{18}) are too soft with the ESP charges, and the stabilization with distributed multipoles shows the importance of anisotropy in the hydrogen bond potential.

Two normal modes (ν_{11}, ν_{20}) twist the molecules approximately around the axis of the N−H···N bond, with minimal distortion of the interchain, edge-to-face contacts. As with the other N−H···N motions, anisotropy in the atom−atom electrostatic interaction increases the frequency of these vibrations. In the quasi-harmonic calculations, the only structural differences between models are small molecular reorientations (1−2° rotations and translations < 0.1 Å), so the differences in frequencies calculated with ESP and DMA models indicate the importance of anisotropy in the hydrogen bond potential.

The remaining vibrations do not distort the hydrogen bonds in the molecular chains but mainly alter the edge-to-face contacts. At the lattice energy minima, the modes corresponding to slipping of these contacts (ν_1, ν_7) are insensitive the model potential and are generally about 10 cm^{-1} too low. The results are improved in the quasi-harmonic calculations, except for the UNI model, where these motions become very soft. Modes that stretch (ν_3) or bend (ν_5, ν_{15}, ν_{19}) the edge-to-face C−H···N contacts are generally too soft with the ESP models, and the DMA stabilizes these interactions.

α-Glycine, $C_2NO_2H_5$. Glycine crystallizes as a zwitterion and three polymorphic modifications are known, the stable room temperature form being the monoclinic ($P2_1/n$) α polymorph. The molecules form double sheets in the crystal (Figure 5), with a network of N−H···O═C hydrogen bonds binding molecules together in layers parallel to the **ac** plane. The molecules have their dipoles aligned within each layer, but pairs of these sheets are arranged antiparallel to each other with further hydrogen bonds joining them. Each hydrogen on the NH_3 group hydrogen bonds to a carbonyl oxygen; both oxygen atoms accept two

TABLE 10: Harmonic and Quasi-harmonic k = 0 Lattice Frequencies of Imidazole

(a) Harmonic $\mathbf{k} = 0$ Lattice Frequencies Calculated at the Minimum in Φ_{latt}, cm^{-1}

mode		expt[a] (100 K, 93 K)	UNI	FIT+ESP	W99+ESP	FIT+DMA	W99+DMA
A_g	ν_1	54.5	44.5	41.2	36.1	45.7	40.3
	ν_2	79.0	62.6	60.0	60.3	79.3	82.5
	ν_3	86.5	63.4	70.1	66.0	98.8	106.3
	ν_4	100.5	106.4	104.6	98.8	111.7	119.4
	ν_5	112.0	162.3	119.7	121.5	141.7	137.1
	ν_6	158.0	168.4	131.6	123.6	213.4	272.9
B_g	ν_7	62.5	64.3	57.6	53.8	54.8	53.6
	ν_8	74.0	72.5	70.4	66.7	86.5	88.4
	ν_9	109.0	110.7	87.8	84.2	108.0	108.0
	ν_{10}	128.0	133.7	111.2	106.0	157.0	169.5
	ν_{11}	163.0	169.8	139.8	132.5	184.1	177.5
	ν_{12}	181.0	183.5	152.0	144.7	206.2	254.0
A_u	ν_{13}	-	74.4	64.2	63.8	74.1	74.0
	ν_{14}	113.0	100.3	83.8	91.7	111.6	104.2
	ν_{15}	-	129.7	113.3	104.9	141.3	161.2
	ν_{16}	151.0	154.4	126.0	119.0	185.3	172.4
	ν_{17}	188.0	183.6	148.3	133.5	198.2	247.9
B_u	ν_{18}	70.0	57.4	44.8	49.4	61.5	69.2
	ν_{19}	97.0	79.1	76.2	73.2	102.3	114.8
	ν_{20}	128.0	105.0	93.1	89.7	149.9	150.5
	ν_{21}	-	177.0	142.3	136.0	209.2	269.4

(b) Quasi-harmonic $\mathbf{k} = 0$ Frequencies in the 103 K Fixed Unit Cell, cm^{-1}

mode		expt [a](100 K, 93 K)	UNI	FIT+ESP	W99+ESP	FIT+DMA	W99+DMA
A_g	ν_1	54.5	36.7	41.1	35.4	44.6	43.8
	ν_2	79.0	74.5	61.9	57.2	83.9	79.5
	ν_3	86.5	102.0	68.7	61.9	94.5	98.7
	ν_4	100.5	113.2	104.5	97.4	126.3	111.4
	ν_5	112.0	140.0	133.7	106.5	147.8	137.0
	ν_6	158.0	166.8	143.5	130.7	208.9	217.4
B_g	ν_7	62.5	20.4	59.4	58.9	61.6	58.0
	ν_8	74.0	58.0	76.1	70.0	83.6	90.3
	ν_9	109.0	92.4	92.7	83.1	116.7	106.8
	ν_{10}	128.0	117.4	117.3	103.2	165.8	127.5
	ν_{11}	163.0	170.2	155.6	132.3	182.6	152.6
	ν_{12}	181.0	188.1	184.9	145.4	205.6	202.2
A_u	ν_{13}	-	50.6	60.4	57.5	81.0	73.1
	ν_{14}	113.0	78.6	90.0	88.8	117.8	114.5
	ν_{15}	-	124.2	120.1	102.2	151.1	128.7
	ν_{16}	151.0	157.9	129.7	108.6	186.8	145.0
	ν_{17}	188.0	180.5	182.9	144.8	202.4	193.0
B_u	ν_{18}	70.0	57.8	42.4	42.0	63.1	70.7
	ν_{19}	97.0	63.2	82.6	72.8	104.1	101.5
	ν_{20}	128.0	131.9	100.1	88.7	158.8	141.4
	ν_{21}	-	143.5	155.2	126.8	210.0	211.8

[a] Raman (A_g, B_g) measured at 100 K, IR (A_u, B_u) at 93 K. Our characterization of the experimental IR modes is based on agreement with our best models (UNI and DMA models in the QH approximation) and is used consistently throughout. However, the number of missing frequencies and the small frequency differences makes this a best estimate rather than a confident assignment.

hydrogen bonds, and one of the hydrogen atoms is bifurcated. There are no strong directional contacts between the double layers.

All model potentials reproduce the room-temperature neutron structure[45] very well (Table 11a,b) and, apart from the UNI model, the calculated lattice energies are also in reasonable agreement with experiment. With molecular orientation as well as the lattice constants taken into account (Table 11a), the DMA potentials perform noticeably better than point charge models and the W99+DMA model gives the best results.

The vibrational spectrum of α-glycine has been studied using polarized Raman and infrared spectroscopy,[46] and isotope shifts of the frequencies, along with lattice dynamical calculations, have been used to characterize the lattice modes.[46,47] The lowest intramolecular modes occur at around 200 cm^{-1} and correspond to COO torsional motions, so the rigid body approximation may affect the higher frequency lattice vibrations, especially those where deformation of the hydrogen bonds is important. In fact, many of the calculated frequencies of modes involving hydrogen bond bending (ν_4, ν_5, ν_{11}, ν_{12}, ν_{16}, ν_{19}, ν_{20}) are too high (Table 12a,b) with the molecules held rigid.

In the lowest two A_u modes (ν_{13}, ν_{14}), the double layers shear across each other, parallel to the **ac**-plane, while the lowest B_u mode (ν_{18}) stretches the interlayer distance. There are no dominant atom−atom interactions between the layers, and the resistance to these motions is fairly independent of the model potential. The stretching frequency is described very well, but the shearing, which is largely dependent on the orientational dependence of these weak interactions, is too soft with all model potentials. The rest of the modes involve deformations of the hydrogen bond network, so are more sensitive to the description of electrostatics. Shearing of the hydrogen bonded sheets (ν_1, ν_2, ν_7, ν_8) is reproduced quite well and, surprisingly, changes in the exp-6 parameters affect these frequencies more than improving the electrostatic model. Stretching of the interlayer hydrogen bonds (ν_3, ν_4, ν_5, ν_9, ν_{12}) is more dependent on the model of electrostatics but is too stiff in all of our calculations. The remaining vibrations distort the interactions within the

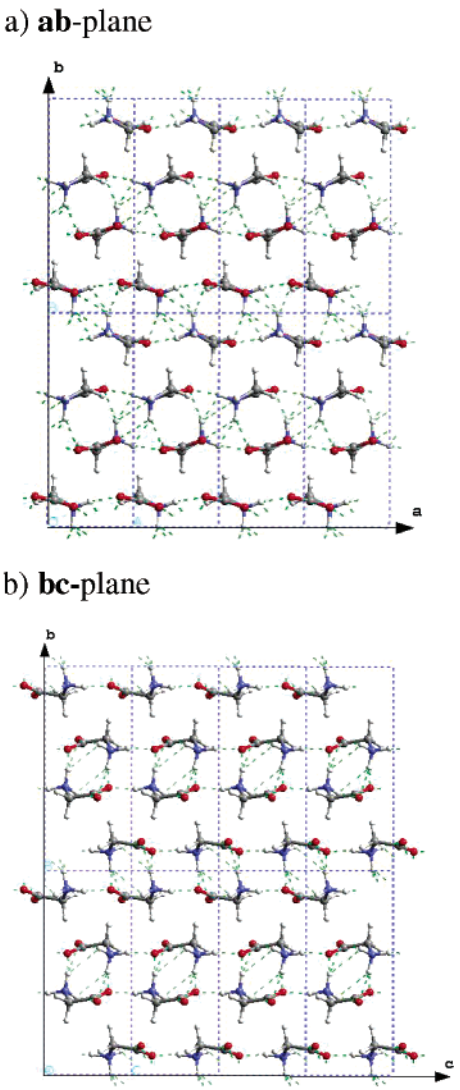

Figure 5. Crystal structure of α-glycine. Hydrogen bonds are shown with fine dashed lines.

molecular layers, and the DMA models generally give higher frequencies; anisotropic atom−atom electrostatics stabilize the hydrogen bond networks, as we found for the other molecular crystals. The overestimation of these frequencies cannot be due to the $T = 0$ K nature of our calculations since the harmonic frequencies are actually lower than the quasi-harmonic calculations corresponding to 295 K. The errors are most likely due to the assumed rigidity around the COO functional groups.

Calculations using the UNI model potential are presented, though the model, with no explicit electrostatics, is not intended for such systems. The errors in lattice parameters are about on par with the point charge models, with only slightly greater molecular reorientations (Table 11b). One translational mode is unstable in the quasi-harmonic approximation. The average errors in the remaining modes are only slightly higher than with the other models, but the errors are less systematic and the order of several modes is reversed.

Thermodynamic Calculations. We calculated sums over the $\mathbf{k} = 0$ frequencies to examine the uncertainties in calculating vibrational contributions to the energy. For the high symmetry hexamethylenetetramine crystal, variations in the only frequency lead directly to changes in the vibrational contributions to the energy. In the other crystals, the errors in the various frequencies have been shown to be very dependent on the nature of the modes and the intermolecular interactions, but it is the overall shape of the calculated spectrum that is important for the energetics. To assess how the errors in the harmonic approximation and model potentials affect the overall vibrational contributions to the energy, two quantities are calculated from each spectrum. Sums of calculated and observed frequencies are compared to estimate errors in the $\mathbf{k} = 0$ contribution to the zero-point energy (Table 13). With increasing temperature, the vibrational energy soon becomes dominated by thermal contributions to the free energy, which are dependent on the logarithm of the partition function, Q, whose vibrational contribution (excluding zero-point contributions)

$$\ln Q_{\mathrm{vib},\mathbf{k}=0} + ZPE/kT = -\sum_i \ln[1 - \exp(-\hbar\omega_i(\mathbf{k}=0)/kT)] \tag{8}$$

has been calculated at the temperatures of the observed spectra (Table 14).

In general, errors in the zero-point energy sum are less than the average errors in the individual frequencies, and the vibrational zero-point energy can be estimated to within 20% in almost all cases, with any choice of these model potentials; the absolute error is well under 1 kJ/mol (Table 13). The zero point energy is dominated by the higher frequencies, so, for example, the quasi-harmonic models of naphthalene, which exaggerate the higher frequencies, have larger errors than at the lattice energy minimum. For the other crystals, the errors in neither the fully relaxed nor quasi-harmonic calculations are consistently lower.

The lowest frequencies are the most important in the partition function, while the effect of the higher frequencies increases with temperature. At very low temperatures, the sum in (8) is nearly zero, so, to judge the quality of the naphthalene and pyrazine low-temperature spectra, the quantity is calculated at 50 K using the low-temperature frequencies. This ignores the temperature dependence of the frequencies, but allows a reasonable comparison between models. Apart from naphthalene, the best model potential for each crystal predicts the sum in (8) to within 5−10%. For naphthalene, the UNI potential gives the best results and, with the W99 models, the low-frequency vibrations are improved in the quasi-harmonic approximation, so the errors are decreased. For pyrazine, the W99+DMA model gives very good agreement with experiment at low temperature and in the quasi-harmonic approximation to room temperature. The advantage of the DMA models is again apparent in the imidazole results. Ignoring molecular flexibility for α-glycine raises the calculated frequencies, increasing the zero-point energy, and decreasing the vibrational partition function. This is apparent in the DMA model calculations. The weaker bonding in the ESP models partly balances this effect, resulting in small errors, especially with the quasi-harmonic calculations.

To give an idea of the thermal energy, one unit of the sum in (8) contributes approximately $8.3/Z$ J/mol·K to the entropy or $2.5/Z$ kJ/mol to the free energy at room temperature, so the typical errors are on the order of 1 kJ/mol at room temperature.

Full calculations of the vibrational contribution to the free energy require the distribution of frequencies over the entire Brillouin zone. We can assume no dispersion of the optic modes (i.e., the frequencies are independent of $\mathbf{k}$) and estimate the significant contribution of the acoustic modes from a Debye model, with a cutoff frequency from the wave velocity, which we calculate from the elastic constants. For the W99+DMA (quasi-harmonic) model, this gives estimated entropies for

TABLE 11: Experimental and Calculated Crystal Structures and Energies and Molecular Displacements for α-Glycine

(a) Experimental and Calculated Crystal Structures and Energies[a]

	$-\Phi_{latt}$ (kJ/mol)	*a* (Å)	*b* (Å)	*c* (Å)	*β* (deg)	vol. (Å^3)	RMS error[c]
expt[45]	223[94, b]	5.10	11.97	5.46	111.7	309.7	
UNI	116.30	*−3.59%*	*−0.82%*	*+1.25%*	*+2.90%*	*−5.51%*	2.25%
FIT+ESP	201.00	*+2.16%*	*+0.46%*	*+1.94%*	*+1.32%*	*+3.51%*	1.70%
W99+ESP	190.76	*+3.94%*	*−0.54%*	*+2.49%*	*−0.41%*	*+6.31%*	2.72%
FIT+DMA	219.06	*−0.71%*	*+1.59%*	*+1.35%*	*+1.06%*	*+1.36%*	1.27%
W99+DMA	206.98	*+0.52%*	*+1.03%*	*+1.76%*	*+0.01%*	*+3.34%*	1.22%

(b) Molecular Displacements During Lattice Energy Relaxation

	Fully relaxed			Fixed cell	
	RMS translation (Å)[d]	RMS rotation (deg)	F	RMS translation (Å)	RMS rotation (deg)
UNI	0.24	4.62	36.69	0.31[c]	5.99[c]
FIT+ESP	0.20	3.71	18.42	0.21	5.04
W99+ESP	0.16	2.88	27.09	0.12	3.75
FIT+DMA	0.25	2.68	14.34	0.21	2.87
W99+DMA	0.14	2.78	8.43	0.11	2.79

[a] Calculated lattice parameters given as % deviations, 100 × (calc − expt)/expt, from experimental values. [b] The experimental lattice energy is estimated by the sublimation enthalpy,[94] corrected by the ab initio energy difference between the classical and zwitterionic gas-phase structures. [c] Root-mean-squared % error on lattice constants. [d] Root-mean-square change of center of mass position on minimization, defined relative to the origin of the unit cell.

naphthalene, α-glycine, and hexamethylenetetramine as 110.07, 76.24, and 101.35 J/mol·K, respectively, which are all much lower than the experimental values of $S° = 167.4$,[95] 103.51,[96] and 163.38 J/mol·K.[97] These errors are greater than those in Table 14 largely because of the importance of the acoustic mode contributions and the typical overestimates of elastic constants.[17] Sampling more points in the Brillouin zone would lessen the reliance on the Debye approximation of acoustic mode contributions and improve the overall accuracy of thermodynamic calculations.

Discussion

Errors in the calculated lattice frequencies are a combination of several approximations in our calculations and, though the effects cannot be completely separated, they are discussed in turn.

Variations in the Model Potential. Differences in functional form and parameterization of the model potential clearly have significant effects on calculated lattice frequencies of molecular organic crystals. Changes in the model potential affect the lattice vibrations directly, through changing the restoring force to the vibrational motion, and indirectly, through changes in the equilibrium structure. Ideally, calculations at the minimum in the lattice energy, with strains on the lattice parameters relaxed, correspond to $T = 0$ K, ignoring the slight changes due to zero-point energy.[98] However, model potentials are often parameterized to ambient temperature properties, so errors in the relaxed structures do not necessarily correspond to thermal effects. When the errors in lattice constants are small (less than 5%), they are not normally considered serious for modeling the structure, but the effects on the calculated lattice vibrations can be important. For example a 1% change in the lattice vector (from 100 K to 298 K) of the hexamethylenetetramine crystal results in changes of more than 10% in the lattice frequency.

The vibrational properties of molecular crystals are sensitive to the shape of the repulsive wall. In the cases where the UNI potential gave good results, this may be due to a more accurate representation of the repulsive wall through the use of explicit parameterization of heteroatomic interactions. Varying the exp-6 parameters with bonding environment contributes to the improvements of the W99 model over the older parameter sets, particularly for the edge-to-face interactions in naphthalene and the vibrations that shear the π-interactions in pyrazine, where aromatic carbon parameters are important. The off-nuclear shift of the hydrogen atom's repulsive wall gives noticeable improvements for vibrations that affect close contacts between nonpolar hydrogen atoms (e.g., naphthalene and pyrazine), but might contribute to the overbonding of strong hydrogen bonds, as in imidazole.

Vibrational motions appear to be more sensitive to the electrostatic interactions than the elastic properties.[17] Generally, anisotropy in the atom−atom model potential is most important for accurate predictions of frequencies involving weak polar interactions and contacts with π−electrons. Also, shearing and bending motions are more dependent on an accurate model potential. Hydrogen bond bending and stretching motions are generally too soft with point charge models, and the more accurate description of electrostatics using distributed multipoles stabilizes these modes. The most extreme example is the pyrazine crystal. Because the two lowest librational modes are nearly pure C−H···N bending, the entire restoring force is due to the orientational dependence of the interaction energy and anisotropic atom−atom interactions are required to keep these modes stable. In the translational modes, where the interaction is stretched as well as bent, the isotropic models are satisfactory.

Quasi-Harmonic Approximation. The quasi-harmonic approximation assumes that anharmonic effects on lattice modes are a result of changes in the lattice constants only, ignoring the modification of frequencies due to the coupling of phonons. In the form that we have implemented such calculations, the lattice vectors are fixed at experimentally observed values. This removes differences in the calculations caused by variations in the relaxed lattice constants. Hence, the calculated frequencies are less sensitive to the model potential in the quasi-harmonic calculations than at the minimum lattice energy structure. Calculating the variation of cell dimensions and molecular positions by free energy minimization (see, e.g., refs 98−101) would remove the reliance on experimental cell parameters. Such calculations have been implemented for hypothetical forms in crystal structure prediction,[7] and we are looking to implement them within DMAREL.

For the cubic hexamethylenetetramine crystal, the effect of varying the lattice on the one optic frequency is easily understood. The frequency shift from 100 K to room temperature

TABLE 12: Harmonic and Quasi-harmonic k = 0 Lattice Frequencies of α-Glycine

(a) Harmonic **k** = 0 Lattice Frequencies at the Minimum in Lattice Energy, cm^{-1}

mode		expt [a]	UNI	FIT+ESP	W99+ESP	FIT+DMA	W99+DMA
A_g	ν_1	52	94.8	67.6	56.8	72.9	52.8
	ν_2	72	58.5	82.4	73.3	79.6	79.8
	ν_3	109	140.8	125.4	122.6	155.9	153.7
	ν_4	155	154.9	135.7	134.1	184.0	179.5
	ν_5	178	276.0	162.6	162.3	192.0	187.7
	ν_6	*194*	208.8	180.5	171.5	233.0	219.6
B_g	ν_7	52	61.9	83.9	82.2	93.9	86.3
	ν_8	73	110.4	91.5	86.5	95.7	94.9
	ν_9	84	134.1	111.1	109.2	146.3	132.7
	ν_{10}	109	162.8	133.2	126.8	173.1	168.6
	ν_{11}	162	184.5	165.5	157.4	200.1	204.3
	ν_{12}	178	274.1	174.1	178.4	231.6	219.2
A_u [(b)]	ν_{13}	91	37.2	49.2	49.7	47.1	50.3
	ν_{14}	91	73.0	56.6	72.2	70.4	70.7
	ν_{15}	- (133)	109.1 (104.4)	80.1 (78.4)	92.0 (87.6)	103.2 (98.4)	125.3 (119.1)
	ν_{16}	- (165)	199.4 (192.8)	141.8 (136.7)	137.1 (131.6)	198.8 (193.1)	190.6 (185.1)
	ν_{17}	*226*	279.5	178.6	160.7	235.3	216.2
B_u	ν_{18}	91	104.3	84.8	90.5	90.4	95.2
	ν_{19}	140	183.2	139.1	136.3	159.1	166.6
	ν_{20}	175	138.2	157.4	150.6	224.1	213.4
	ν_{21}	not observed	279.9	209.2	197.8	239.3	223.5

(b) Quasi-harmonic **k** = 0 Lattice Frequencies of α-Glycine in the Room-Temperature Lattice, cm^{-1}

mode		expt[a]	UNI	FIT+ESP	W99+ESP	FIT+DMA	W99+DMA
A_g	ν_1	52	44.1	72.4	66.6	73.3	57.1
	ν_2	72	62.5	86.0	77.8	77.4	81.5
	ν_3	109	148.4	130.5	125.3	157.3	162.8
	ν_4	155	170.8	144.1	158.2	184.8	182.6
	ν_5	178	211.2	163.8	164.6	192.9	192.3
	ν_6	*194*	253.8	187.8	189.6	226.2	230.2
B_g	ν_7	52	71.6	87.9	86.5	93.3	94.8
	ν_8	73	79.5	89.1	87.2	102.0	97.2
	ν_9	84	125.1	119.2	116.3	150.6	139.7
	ν_{10}	109	160.2	140.0	145.9	172.0	173.0
	ν_{11}	162	176.7	167.6	172.7	197.2	206.1
	ν_{12}	178	252.2	175.3	182.9	222.6	229.5
A_u[b]	ν_{13}	91	**−77.1**	51.9	51.7	49.6	51.8
	ν_{14}	91	48.3	70.5	80.9	78.2	78.8
	ν_{15}	− (133)	58.5 (57.2)	84.9 (83.3)	97.9 (93.5)	103.8 (99.0)	130.3 (123.7)
	ν_{16}	− (165)	93.5 (89.0)	146.3 (141.3)	147.5 (142.8)	192.4 (187.1)	193.8 (188.4)
	ν_{17}	*226*	186.0	183.0	184.0	228.1	227.8
B_u	ν_{18}	91	87.0	95.5	104.6	97.7	106.8
	ν_{19}	140	207.7	150.2	148.0	166.5	174.8
	ν_{20}	175	252.1	167.4	179.7	213.2	219.5
	ν_{21}	not observed	272.7	212.3	202.9	234.8	229.7

[a] Characterization of the frequencies in italics as lattice modes was uncertain.[46,47] Frequencies given in parentheses are for the N-deuterated crystal.

is reproduced very well in the quasi-harmonic approximation. With the W99+DMA model, the difference in frequency between the 100 K and room temperature quasi-harmonic calculations follows experiment very closely. The low temperature structure is also reproduced very well with this model potential, so the frequency difference between the fully relaxed and 100 K quasi-harmonic calculations is probably a good approximation for the real difference between 0 K and 100 K frequencies. With the less symmetrical crystals, the differences between frequencies calculated in the fully relaxed structures and in the fixed lattice are less straightforward. It is apparent in some cases that small changes in the lattice constants are needed to optimize the close contacts between the molecules. This is true in pyrazine, where the anisotropy of the C−H···N contacts is important. In the relaxed lattice, the directionality of the interaction is optimized, but the fixed unit cell hinders optimal orientation of the weak hydrogen bonds. Similarly, in the UNI model imidazole calculations, where the edge-to-face interactions contract significantly when the lattice is relaxed, fixing the unit cell keeps the interactions farther apart and the shearing motions of these contacts become soft.

Anharmonic modifications of the frequencies, which are ignored in the quasi-harmonic model, are expected to be less important at moderate temperatures. The phonon anharmonicity in naphthalene has been studied both computationally[31] and experimentally[23,77] by measuring frequency shifts with temperature and pressure. These studies show that the shift varies considerably between modes and that the anharmonicity increases the frequencies of the intermolecular phonons by less than 3 cm^{-1} (at $T = 0$ K).

Rigid Body Approximation. The cage structure in hexamethylenetetramine and π-delocalization in naphthalene, pyrazine, and imidazole give considerable rigidity to these molecules, so the effects of intramolecular deformation on the lattice frequencies are likely to be similar for these molecules and smaller than for most organic molecules. Pawley and Cyvin[25] estimated that molecular deformations can lower the calculated frequencies of naphthalene by 5−10 cm^{-1}. This error is

TABLE 13: Comparison of Estimates of the Zero-Point Vibrations ($\hbar/2)\sum_i \omega_i$ ($\mathbf{k} = 0$) in kJ/mol[a]

expt		UNI	FIT+ESP	W99+ESP	FIT+DMA	W99+DMA
naphthalene, 6 K[b]						
2.30	fully relaxed	2.48 (+7.9%)	2.30 (+0.2%)	2.16 (−5.9%)	2.34 (+1.9%)	2.20 (−4.2%)
	QH	2.5 (+10.7%)	2.93 (+27.6%)	2.67 (+16.2%)	2.95 (+28.5%)	2.69 (+16.9%)
Pyrazine						
2.09, Low T[c]	fully relaxed				2.14 (+2.5%)	2.17 (+3.9%)
1.73, RT[d]	QH				1.88 (+9.0%)	1.88 (+8.5%)
imidazole, 100K						
3.07	fully relaxed	3.02 (−1.6%)	2.57 (−16.4%)	2.47 (−19.7%)	3.43 (+11.7%)	3.69 (+20.1%)
	QH	2.92 (−5.1%)	2.79 (−9.1%)	2.47 (−19.8%)	3.52 (+14.6%)	3.28 (+6.6%)
α-glycine, RT[e]						
3.78	fully relaxed		3.58 (−5.4%)	3.50 (−7.5%)	4.45 (+17.6%)	4.33 (+14.5%)
	QH		3.75 (−0.9%)	3.83 (+1.1%)	4.44 (+17.4%)	4.51 (+19.3%)

[a] The frequencies that are missing from the experimental spectrum are also left out of the sums for the calculated spectra. [b] The experimental (4.7 K) and calculated values for the undeuterated B_u frequency are included in the sum. [c] The IR and Raman were measured at different temperatures, but we have included them in the same sum for comparison with our calculations. [d] The room temperature IR spectrum was only available for the fully deuterated crystal, so the experimental and calculated sums include both h_4 and d_4 frequencies. [e] Calculated frequencies for the N-deuterated crystal are used for the two A_u modes for which there is only experimental data for the N-deuterated crystal.

TABLE 14: Vibrational Contribution to $\ln Q_{vib,k=0} + {}^{ZPE}/_{kT} = -\sum_i \ln[1 - \exp(-\hbar\omega_i(\mathbf{k} = 0)/kT)]$ (dimensionless)[a]

expt		UNI	FIT+ESP	W99+ESP	FIT+DMA	W99+DMA
naphthalene, 50 K[b]						
1.04	fully relaxed	1.09 (+4.8%)	1.27 (+22.1%)	1.39 (+33.7%)	1.25 (+20.2%)	1.41 (+35.6%)
	QH	0.97 (−6.7%)	0.72 (−30.8%)	0.89 (−14.4%)	0.73 (−29.8%)	0.90 (−13.5%)
pyrazine						
0.96 (50 K[c])	fully relaxed				1.13 (+17.2%)	0.99 (+3.4%)
10.22 (298K [d])	QH				11.15 (+9.1%)	10.00 (−2.2%)
hexamethylenetetramine						
0.51 (100 K)	fully relaxed	0.29 (−43%)	0.39 (−24%)	0.42 (−17%)	0.49 (−5%)	0.59 (+15%)
	QH	0.42 (−17%)	0.34 (−34%)	0.43 (−15%)	0.43 (−17%)	0.59 (+16%)
1.40 (298 K)	QH	1.34 (−4.5%)	1.17 (−17%)	1.31 (−6.5%)	1.31 (−6.5%)	1.54 (+9.4%)
imidazole, 100 K[e]						
4.79	fully relaxed	5.38 (+12.3%)	6.38 (+33.2%)	6.68 (+39.5%)	4.49 (−6.3%)	4.35 (−9.2%)
	QH	6.46 (+34.9%)	5.98 (+24.8%)	6.76 (+41.3%)	4.28 (−10.6%)	4.58 (−4.4%)
α-glycine, RT[f]						
17.32	fully relaxed		17.83 (+2.9%)	18.05 (+4.2%)	15.32 (−11.5%)	15.67 (−9.5%)
	QH		17.01 (−1.8%)	16.78 (−3.1%)	15.15 (−12.5%)	15.00 (−13.4%)

[a] The frequencies that are missing from the experimental spectrum are also left out of the sums for the calculated spectra. [b] Calculated using the 6 K experimental and calculated frequencies. [c] Calculated at 50 K using the low-temperature spectra (Raman measured at 4.2 K, IR at 77 K) and the mode with no experimental observation was left out of the calculation. [d] The room temperature IR spectrum is only available for the fully deuterated crystal, so the experimental and calculated values of the h_4 translational mode frequencies are included in the sum. [e] The IR and Raman frequencies are measured at different temperatures (93 K and 100 K, respectively), but we have included them in the same sum and used 100 K in the calculations. [f] Calculated frequencies for the N-deuterated crystal are used for the two A_u modes for which there is only experimental data for the N-deuterated crystal.

significant and similar to the variations in the frequencies calculated with the more accurate intermolecular potentials. Hence, further force-field improvements are limited by the rigid body assumption. Glycine is expected to be somewhat more flexible and low energy torsions of the COO group are a likely source of the errors in the high-frequency deformations of hydrogen bonding.

Conclusions

The $\mathbf{k} = 0$ phonon frequencies of five molecular organic crystals have been calculated by standard lattice dynamical methods. A second-derivative method for rigid molecules has been implemented in the crystal structure modeling program DMAREL,[65] allowing the use of anisotropic atom−atom model

potentials and therefore high accuracy electrostatic models. The present work addresses the sensitivity of such calculations to changes in the form and parameterization of the model potential.

The lattice dynamics of molecular crystals is determined mainly by the close contacts, so the quality of the repulsion-dispersion model is important. Point charge electrostatic models are often not sufficient to describe vibrations that bend or shear polar interactions. A distributed multipole description of the electrostatics stabilizes these motions. For weak polar interactions and the shearing of contacts with aromatic rings, the anisotropic atom−atom models give the best agreement with observed spectra. These modes are generally in the lower frequency part of the spectrum, and so make a dominant contribution to the partition function, particularly at low temperatures. For stronger hydrogen bonded systems, a carefully parameterized exp-6 model with no explicit electrostatics (such as UNI) can give comparable results to the more complex models.

Although individual frequencies can have errors that may present difficulties in characterizing the complex spectra of most low-symmetry organic crystals, statistical properties are less sensitive to the details of the spectra. Zone-center optic mode contributions to zero-point energies and the vibrational partition function can be calculated to within 20% and 10%, respectively, with the best model potentials. Thus, such calculations should give reasonable estimates for these contributions to thermodynamical functions of molecular organic crystals when anharmonic effects and the coupling to intramolecular modes are small. However, good estimates of acoustic mode dispersion or sampling of more points in the Brillouin zone are needed for accurate thermodynamic calculations. In addition to this limitation, the variation in the quality of calculations between the very different molecules studied is sufficiently small that these thermodynamic quantities can be quite confidently compared for different crystal structures of the same molecule. Hence, these calculations should be useful for predicting the low-temperature behavior of molecular materials.

Acknowledgment. G.M.D. was supported by UCL Graduate School, ORS, and NSERC scholarships, and the work was carried out in collaboration with an EPSRC ROPA grant.

Supporting Information Available: Tables of qualitative descriptions of calculated vibrational modes for naphthalene, pyrazine, imidazole, and α-glycine. This material is available free of charge via the Internet at http://pubs.acs.org.

References and Notes

(1) Grunenberg, A.; Henck, J. O.; Siesler, H. W. *Int. J. Pharm.* **1996**, *129*, 147.
(2) Grant, D. J. W. Theory and Origin of Polymorphism. In *Polymorphism in Pharmaceutical Solids*; Brittain, H. G., Ed.; Marcel Dekker Inc.: New York, 1999; p 1.
(3) Bernstein, J. *Polymorphism in Molecular Crystals*; Clarendon Press: Oxford, 2002.
(4) Dunitz, J. D.; Bernstein, J. *Acc. Chem. Res.* **1995**, *28*, 193.
(5) Gavezzotti, A.; Filippini, G. *J. Am. Chem. Soc.* **1995**, *117*, 12299.
(6) Dunitz, J. D.; Filippini, G.; Gavezzotti, A. *Helv. Chim. Acta* **2000**, *83*, 2317.
(7) van Eijck, B. P. *J. Comput. Chem.* **2001**, *22*, 816.
(8) van Eijck, B. P.; Mooij, W. T. M.; Kroon, J. *J. Phys. Chem. B* **2001**, *105*, 10573.
(9) Anghel, A. T.; Day, G. M.; Price, S. L. *CrystEngComm* **2002**, *4*, 348.
(10) Lewis, T. C.; Tocher, D. A.; Day, G. M.; Price, S. L. *CrystEngComm* **2003**, *5*, 3.
(11) Filippini, G.; Gavezzotti, A. *Acta Crystallogr.* **1993**, *B49*, 868.
(12) Gavezzotti, A.; Filippini, G. *J. Phys. Chem.* **1994**, *98*, 4831.
(13) Dunitz, J. D. *Chem. Commun.*. **2003**, 545.
(14) Della Valle, R. G.; Venuti, E.; Brillante, A. *J. Chem. Phys.* **2003**, *118*, 807.
(15) Williams, D. E. *J. Chem. Phys.* **1966**, *45*, 3770.
(16) Bonadeo, H.; D'Alessio, E. In *Lattice Dynamics and Intermolecular Forces*; Corso, L. V., Ed.; Academic Press: New York, 1975; pp 136.
(17) Day, G. M.; Price, S. L.; Leslie, M. *Cryst. Growth Des.* **2000**, *1*, 13.
(18) Kampermann, S. P.; Sabine, T. M.; Craven, B. M.; McMullan, R. K. *Acta Crystallogr.* **1995**, *A51*, 489.
(19) Dolling, G.; Powell, B. M. *Proc. Royal Soc. London, A* **1970**, *319*, 209.
(20) Cochran, W.; Pawley, G. S. *Proc. Royal Society* **1964**, *A280*, 1.
(21) Powell, B. M.; Sándor, E. *J. Phys. C: Solid State Phys.* **1971**, *4*, 23.
(22) Natkaniec, I.; Belushkin, A. V.; Dyck, W.; Fuess, H.; Zeyen, C. M. E. *Z. Kristallogr.* **1983**, *163*, 285.
(23) Sheka, E. F.; Bokhenkov, E. L.; Dorner, B.; Kalus, J.; Mackenzie, G. A.; Natkaniec, I.; Pawley, G. S.; Schmelzer, U. *J. Phys. C: Solid State Phys.* **1984**, *17*, 5893.
(24) Pawley, G. S. *Phys. Status Solidi* **1967**, *20*, 347.
(25) Pawley, G. S.; Cyvin, S. J. *J. Chem. Phys.* **1970**, *52*, 4073.
(26) Mackenzie, G. A.; Pawley, G. S.; Dietrich, O. W. *J. Phys. C: Solid State Phys.* **1977**, *10*, 3723.
(27) Pawley, G. S.; Mackenzie, G. A.; Bokhenkov, E. L.; Sheka, E. F.; Dorner, B.; Kalus, J.; Schmelzer, U.; Natkaniec, I. *Mol. Phys.* **1980**, *39*, 251.
(28) Della Valle, R. G.; Venuti, E.; Brillante, A. *Chem. Phys.* **1995**, *198*, 79.
(29) Righini, R.; Califano, S.; Walmsley, S. H. *Chem. Phys.* **1980**, *50*, 113.
(30) Righini, R. *Physica B & C* **1985**, *131*, 234.
(31) Jindal, V. K.; Kalus, J. *J. Phys. C: Solid State Phys.* **1983**, *16*, 3061.
(32) Kalus, J. *J. Chim. Phys. Phys.-Chim. Biol.* **1985**, *82*, 137.
(33) Pertsin, A. J.; Kitaigorodskii, A. I. *The Atom-Atom Potential Method. Applications to Organic Molecular Solids*; Springer-Verlag: Berlin, 1987.
(34) Wheatley, P. J. *Acta Crystallogr.* **1957**, *10*, 182.
(35) de With, G.; Harkema, S.; Feil, D. *Acta Crystallogr.* **1976**, *B32*, 3178.
(36) Gerbaux, X.; Hadni, A. *J. Chem. Phys.* **1968**, *49*, 955.
(37) Hieida, T.; Maehara, M.; Nibu, Y.; Shimada, H.; Shimada, R. *Bull. Chem. Soc. Jpn.* **1989**, *62*, 925.
(38) Reynolds, P. A. *J. Chem. Phys.* **1973**, *59*, 2777.
(39) Ito, M.; Shigeoka, T. *J. Chem. Phys.* **1966**, *44*, 1001.
(40) Gamba, Z.; Bonadeo, H. *J. Chem. Phys.* **1981**, *75*, 5059.
(41) Gamba, Z. *J. Chem. Phys.* **1989**, *91*, 1697.
(42) McMullan, R. K.; Epstein, K.; Ruble, J. R.; Craven, B. M. *Acta Crystallogr.* **1979**, *B35*, 688.
(43) Perchard, C.; Novak, A. *J. Chem. Phys.* **1968**, *48*, 3079.
(44) Majoube, M.; Vergoten, G. *J. Chem. Phys.* **1982**, *76*, 2838.
(45) Power, L. F.; Turner, K. E.; Moore, F. H. *Acta Crystallogr.* **1976**, *B32*, 11.
(46) Machida, K.; Kagayama, A.; Saito, Y.; Kuroda, Y.; Uno, T. *Spectrochim. Acta* **1977**, *33A*, 569.
(47) Machida, K.; Kagayama, A.; Kuroda, Y. *Bull. Chem. Soc. Jpn.* **1981**, *54*, 1348.
(48) Allen, F. H.; Kennard, O.; Watson, D. G.; Brammer, L.; Orpen, A. G. *J. Chem. Soc., Perkin Trans. 2* **1987**, S1.
(49) Price, S. L. In *Reviews in Computational Chemistry*; Lipkowitz, K. B., Boyd, D. B., Eds.; Wiley-VCH: John Wiley and Sons: New York, 2000; Vol. 14; pp 225.
(50) Williams, D. E.; Starr, T. L. *Comput. Chem.* **1977**, *1*, 173.
(51) Cox, S. R.; Hsu, L.-Y.; Williams, D. E. *Acta Crystallogr.* **1981**, *A37*, 293.
(52) Williams, D. E.; Cox, S. R. *Acta Crystallogr.* **1984**, *B40*, 404.
(53) Coombes, D. S.; Price, S. L.; Willock, D. J.; Leslie, M. *J. Phys. Chem.* **1996**, *100*, 7352.
(54) Beyer, T.; Price, S. L. *J. Phys. Chem. B* **2000**, *104*, 2647.
(55) Williams, D. E. *J. Mol. Struct.* **1999**, *486*, 321.
(56) Williams, D. E. *J. Comput. Chem.* **2001**, *22*, 1154.
(57) Williams, D. E. *J. Comput. Chem.* **2001**, *22*, 1.
(58) Frisch, M. J.; Trucks, G. W.; Schlegel, H. B.; Scuseria, G. E.; Robb, M. A.; Chesseman, J. R.; Zakrzewski, V. G.; Montgomery, J. A.; Stratmann, R. E.; Burant, J. C.; Dapprich, S.; Millam, J. M.; Daniels, A. D.; Kudin, K. N.; Strain, M. C.; Farkas, O.; Tomasi, J.; Barone, V.; Cossi, M.; Cammi, R.; Mennucci, B.; Pomelli, C.; Adamo, C.; Clifford, S.; Ochterski, J.; Petersson, G. A.; Ayalla, P. Y.; Cui, Q.; Morokuma, K.; Malick, D. K.; Rabuck, A. D.; Raghavachari, K.; Foresman, J. B.; Cioslowski, J.; Ortiz, J. V.; Stefanov, B. B.; Liu, G.; Liashenko, A.; Piskorz, P.; Komaromi, I.; Gomperts, R.; Martin, R. L.; Fox, D. J.; Keith, T.; Al-Laham, M. A.; Peng, C. Y.; Nanayakkara, A.; Gonzalez, C.; Challacombe, M.; Gill, P. M. W.; Johnson, B. G.; Chen, W.; Wong, M. W.; Andres, J. L.; Head-Gordon, M.;

Replogle, E. S.; Pople, J. A. Gaussian 98; Revision A.6 ed.; Gaussian Inc.: Pittsburgh, 1998.
(59) Breneman, C. M.; Wiberg, K. B. *J. Comput. Chem.* **1990**, *11*, 361.
(60) Stone, A. J. *Chem. Phys. Lett.* **1981**, *83*, 233.
(61) Stone, A. J.; Alderton, M. *Mol. Phys.* **1985**, *56*, 1047.
(62) Stone, A. J. GDMA: Distributed Multipole Analysis of Gaussian Wavefunctions; 1.0 ed.; University of Cambridge.
(63) Price, S. L.; Stone, A. J.; Alderton, M. *Mol. Phys.* **1984**, *79*, 987.
(64) Popelier, P. L. A.; Stone, A. J. *Mol. Phys.* **1994**, *82*, 411.
(65) Willock, D. J.; Price, S. L.; Leslie, M.; Catlow, C. R. A. *J. Comput. Chem.* **1995**, *16*, 628.
(66) Ewald, P. *Ann. Phys.* **1921**, *64*, 253.
(67) Born, M.; Huang, K. *Dynamical Theory of Crystal Lattices*; Oxford University Press: New York, 1954.
(68) Walmsley, S. H. In *Phonons in Molecular Crystals*; Zahlan, A. B., Ed.; University Press: Cambridge, 1968; pp 83.
(69) Walmsley, S. H. In *Lattice Dynamics and Intermolecular Forces*; Corso, L. V., Ed.; Academic Press: New York, 1975; pp 81.
(70) Califano, S.; Schettino, V.; Neto, N. *Lattice Dynamics of Molecular Crystals*; Springer-Verlag: Berlin, 1981; Vol. 26.
(71) Dove, M. T. *Introduction to Lattice Dynamics*; Cambridge University Press: Cambridge, 1993.
(72) Day, G. M.; RUDOLPh. A program for visualising phonon modes in rigid molecular crystals.; 1.0 ed. London, 2001.
(73) Cerius2; Molecular Simulations Inc.: San Diego, 1997.
(74) Mansson, M.; Rapport, N.; Westrum, E. F., Jr. *J. Am. Chem. Soc.* **1970**, *92*, 7296.
(75) Stevens, E. D.; Hope, H. *Acta Crystallogr.* **1975**, *A31*, 494.
(76) Pertsin, A. J. *J. Phys. Chem. Solids* **1985**, *46*, 1019.
(77) Schmelzer, U.; Bokhenkov, E. L.; Dorner, B.; Kalus, J.; Mackenzie, G. A.; Natkaniec, I.; Pawley, G. S.; Sheka, E. F. *J. Phys. C: Solid State Phys.* **1981**, *14*, 1025.
(78) Gavezzotti, A. *Theoretical Aspects and Computer Modelling of the Molecular Solid State*; John Wiley & Sons: Chichester, 1997.
(79) Williams, D. E. PCK83; QCPE Program 548. Quantum Chemistry Program Exchange: Chemistry Department, Indiana University, Bloomington, Indiana, 1983.
(80) Brock, C. P.; Dunitz, J. D. *Acta Crystallogr.* **1982**, *B38*, 2218.
(81) Miller, G. A. *J. Chem. Eng. Data* **1963**, *8*.
(82) Colomina, M.; Jimenez, P.; Turrion, C. *J. Chem. Thermodyn.* **1982**, *14*, 779.
(83) Gluchova, O. T.; Skljarevskij, O. I.; Janson, I. K.; Teplickij, A. B. *Zh. Fiz. Khim.* **1982**, *56*, 1535.
(84) Murata, S.; Sakiyama, M.; Seki, S. *J. Chem. Thermodyn.* **1982**, *14*, 707.
(85) Holdiness, M. R. *Thermochim. Acta* **1983**, *71*, 257.
(86) Torres-Gomez, L. A.; Barreiro-Rodriguez, G.; Galarza-Mondragon, A. *Thermochim. Acta* **1988**, *124*, 229.
(87) Chirico, R. D.; Knipmeyer, S. E.; Nguyen, A.; Steele, W. V. *J. Chem. Thermodyn.* **1993**, *25*, 1461.
(88) Chickos, J.; Hesse, D.; Hosseini, S.; Nichols, G.; Webb, P. *Thermochim. Acta* **1998**, *313*, 101.
(89) Price, S. L. *Chem. Phys. Lett.* **1985**, *114*, 359.
(90) Suzuki, M.; Yokoyama, H.; Ito, M. *Spectrochim. Acta* **1968**, *24A*, 1091.
(91) Tjebbes, J. *Acta Chem. Scand.* **1962**, *62*, 916.
(92) Gamba, Z. *J. Chem. Phys.* **1985**, *83*, 5892.
(93) Jiminez, P.; Roux, M. V.; Turrioun, C. *J. Chem. Thermodyn.* **1987**, *19*, 985.
(94) Gaffney, J. S.; Pierce, R. C.; Friedman, L. *J. Am. Chem. Soc.* **1977**, *99*, 4293.
(95) McCullough, J. P.; Finke, H. L.; Messerly, J. F.; Kincheloe, T. C.; Waddington, G. *J. Phys. Chem.* **1957**, *61*, 1105.
(96) Hutchens, J. O.; Cole, A. G.; Stout, J. W. *J. Am. Chem. Soc.* **1960**, *82*, 4813.
(97) Westrum, E. F., Jr. *J. Phys. Chem. Solids* **1961**, *18*, 83.
(98) Filippini, G.; Gramaccioli, C. M. *Acta Crystallogr.* **1981**, *A37*, 335.
(99) Allan, N. L.; Barron, T. H. K.; Bruno, J. A. O. *J. Chem. Phys.* **1996**, *105*, 8300.
(100) Taylor, M. B.; Barrera, G. D.; Allan, N. L.; Barron, T. H. K. *Phys. Rev. B* **1997**, *56*, 380.
(101) Allan, N. L.; Barrera, G. D.; Barron, T. H. K.; Taylor, M. B. *Int. J. Thermophysics* **2001**, *22*, 535.